Catalysis Letters (2021) 151:1080–1090
https://doi.org/10.1007/s10562-020-03370-1

The Sintering of Au Nanoparticles on Flat {100}, {111} and Zigzagged {111}-Nanofacetted Structures of Ceria and Its Influence on Catalytic Activity in CO Oxidation and CO PROX

O. S. Bezkrovnyi[1] · P. Kraszkiewicz[1] · W. Mista[1] · L. Kepinski[1]

Received: 21 April 2020 / Accepted: 28 August 2020 / Published online: 8 September 2020

Abstract
The thermal stability of Au nanoparticles on ceria support of various morphology (nanocubes, nanooctahedra, and {111}-nanofacetted nanocubes) in oxidizing and reducing atmospheres was investigated by electron microscopy. A beneficial effect of the reconstruction of edges of ceria nanocubes into zigzagged {111}-nanofacetted structures on the inhibition of sintering of Au nanoparticles was shown. The influence of different morphology of Au particles on various ceria supports on the reducibility and catalytic activity in CO oxidation, and CO PROX of Au/ceria catalysts was also investigated and discussed. It was shown, that ceria nanocubes with flat {110} terminated edges are more suitable as a support for Au nanoparticles, used to catalyze CO oxidation, than zigzagged {111}- nanofacetted structures.

Graphic Abstract

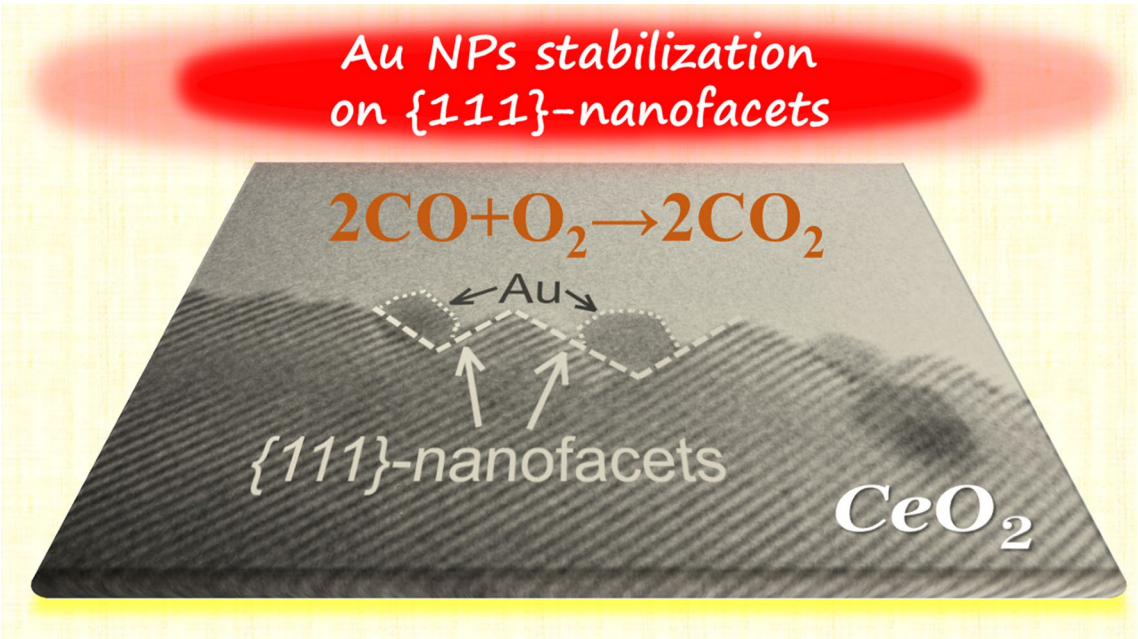

Keywords Ceria support · Nanofacetes · Au nanoparticles · Sintering · H_2-TPR · Co–oxidation · CO PROX

Electronic supplementary material The online version of this article (https://doi.org/10.1007/s10562-020-03370-1) contains supplementary material, which is available to authorized users.

Extended author information available on the last page of the article

1 Introduction

As a reducible oxide with facile oxygen vacancy formation and easy conversion between the Ce^{3+} and Ce^{4+} oxidation states, ceria displays good characteristics both as a catalyst and «active» catalytic support [1]. High efficiency of ceria as active support for noble metal catalysts can be explained by the effective supply of oxygen from ceria to noble metal nanoparticle to form active oxidic sites [2]. Theoretical DFT calculations by Conesa showed that the energy of the formation of oxygen vacancies is structure-sensitive, following the sequence {110} < {100} < {111} [3]. Molecular dynamics (MD) calculations by Castanet et al. showed that the surface oxygen mobility on {100} surfaces of CeO_2 is one and five orders higher than that on the {110} and {111} surfaces, respectively [4]. It explains, why cube-shape ceria nanoparticles (mainly terminated by {100} faces) are preferable for catalytic applications then nanoparticles with irregular shape or nanooctahedra (mainly terminated by {111} faces) [1].

Gold atoms at the perimeter of the gold nanoparticles deposited on active support play the primary role in catalysis of Red-Ox reactions (e.g., CO oxidation) [5]. So the sintering of gold nanoparticles at elevated temperatures (at working conditions) will result in a severe decline of the catalytic activity of Au/ceria composite. An inhibition of gold nanoparticles growth at elevated temperatures is, therefore, a very urgent task considering the possible application of Au/ceria nanocomposite materials in practice.

Up to now, several strategies have been proposed to increase the stability of Au NPs at elevated temperatures. One method of increasing the sintering resistance of gold nanoparticles is to anchor them on the surface of the support by strengthening the metal-support interaction. Ta et al., proposed a mechanism of gold nanoparticles stabilization on ceria nanorods, according to which gold atoms at the metal-support interface are anchored onto the underlying surface oxygen vacancies on cerium oxide. They showed that bonding between the surface oxygen vacancies and the gold particles is so strong, that the particles could only rotate/vibrate locally, but could not migrate to form aggregates.[6]. The number of oxygen vacancies at ceria surface—potential sites for anchoring gold nanoparticles—can be controlled by the type of thermal treatment atmosphere (oxidizing or reducing) and, as we mentioned above, by type of CeO_2 surface—{100}, {110} or {111}. In our study, we investigated the sintering of Au nanoparticles supported by nanocubes (mainly terminated by {100} faces) and nanooctahedra (terminated by {111} faces) in the both oxidative and reducible atmosphere.

Another approach to inhibit sintering of gold nanoparticles is to fix them inside the pores of the support [7] or to encapsulate them with thin shells of porous oxide [8, 9]. This approach is based on the geometrical immobilization of Au nanoparticles, which inhibits both possible sintering mechanisms—"Particle migration" [10, 11] and "Ostwald ripening" [11]. However, the "encapsulation" strategy may result in a covering of the active sites and restrict reagents access to them, which can reduce the catalytic activity of such materials.

It appears that the disadvantages of the above method of stabilization can be overcome by using support with a zigzagged nano-facetted surface, where both sintering mechanisms will be inhibited due to geometric constraints, while free access of reagents to active sites will be maintained.

Theoretical DFT calculations by Fronzi et al. showed that {110}-CeO_2 surface is metastable and tends to reconstruct into {111}-related structures [12]. MD calculations by Castanet et al. showed thermally induced reconstruction of {110} edges of ceria nanocubes into zigzagged {111}-nanfacetted structures [4]. It was confirmed experimentally in several publications [4, 13–16], that the {110} edges of ceria nanocubes transform into a set of nanometer-height, {111}—bounded facets as a result of treatment at 500–600 °C. Even though nanocubes' edges (exposing flat {110} face or {111} nanofacets) make < 10% of the total surface area, they have a decisive effect on the reactivity of CeO_2 and Au/CeO_2 catalysts in CO oxidation [13, 14]. Despite a promising perspective of using such textured ceria nanoparticles as active supports for noble metal catalysts, there are no publications devoted to the thermal stability of Au on such structures.

The present study aims at determining the role of the morphology of ceria support (nanocubes, nanooctahedra, and zigzagged {111}-nanofacetted ceria nanocubes) and type of atmosphere on the thermal stability of Au nanoparticles—key factor responsible for the efficiency and stability of Au/ceria-based catalysts at elevated temperatures. Moreover, reducibility, catalytic activity, and selectivity of these materials in the CO oxidation and CO PROX were also investigated and discussed.

2 Experimental Section

Nanocubes (CeO_2(NC)) and nanooctahedra (CeO_2(NO)) of ceria were synthesized by the microwave-assisted hydrothermal method [17–19]. $Ce(NO_3)_3$ was first dissolved in distilled water. Next, the obtained solution was mixed with an appropriate amount of aqueous sodium hydroxide (NaOH) solution (for cube-shape crystals) or sodium phosphate (Na_3PO_4) solution (for octahedral crystals) and then stirred for 60 min. The final solution was treated at 200 °C or 170 °C for 3 h under autogenous pressure in an autoclave to obtain cube-shape and octahedral nanocrystals,

respectively. The as-obtained precipitate powder was washed and dried at 60 °C for 12 h. {111}-nanofacetted nanocubes (CeO_2(NF)) were prepared by annealing of smooth ceria nanocubes (CeO_2(NC)) in H_2 atmosphere at 500 °C for 3 h, and additional annealing at 200 °C/2 h in O_2 (5%) + He (95%)) [14].

Au nanoparticles were deposited on the ceria nanocubes using a wet chemical deposition–precipitation method similar to that used by Lin et al. [20]. 200 mg of ceria support, 8 mg of $H[AuCl_4]$, 512 mg of $(NH_2)_2CO$, and 12 mL of H_2O were mixed to form a suspension. The suspension was stirred and kept at 80 °C in a silicone oil bath for 24 h. Au/ceria particles were washed, dried at 50 °C for 12 h, and annealed in air (or in H_2) at 300 °C or 500 °C for 3 h.

The crystal structure and morphology of the samples were determined by transmission electron microscopy (TEM), using a Philips CM-20 SuperTwin instrument operating at 160 kV. Chemical composition and element distribution in the samples were checked with an FEI NovaNanoSEM 230 equipped with EDAX Genesis XM4 detector, and inductively coupled plasma (ICP) techniques. Specific surface area (SSA) was measured with a Micromeritics ASAP 2020 C instrument at—196 °C. The surface area was calculated using the Brunauer–Emmett–Teller (BET) method. The reducibility of the samples was tested with H_2-TPR (temperature-programmed reduction) technique by heating the samples (50 mg) with a heating rate of 10 °C min^{-1} up to 900 °C in H_2 (5 vol.%)/Ar flow. The hydrogen consumption was monitored by a thermal conductivity detector (TCD) (Autochem II 2920, Micromeritics).

The catalytic activity of the samples was tested in CO oxidation and CO PROX. Typically, 50 mg of catalyst was placed in the quartz microreactor (Autochem II 2920, Micromeritics). The gas stream containing 1% CO, 5% O_2 or 1% CO, 1% O_2 and 40%H_2, balanced with He (total flow rate 50 cm^3min^{-1}) for CO oxidation and CO-PROX, respectively, was introduced into the reactor at—50 °C and the light-off curves were obtained with a temperature ramp rate of 3 °C/min. The outlet gas composition was analyzed by a mass spectrometer (OmniStar QMS-200, Pfeiffer Vacuum) calibrated with gas mixtures of known composition. CO conversion (CO_{conv}) and selectivity to CO_2 (S_{CO2}) were calculated as follows:

$$CO_{conv}[\%] = \frac{CO_{in} - CO_{out}}{CO_{in}} \times 100\%$$

$$S_{CO_2}[\%] = \frac{CO_{in} - CO_{out}}{2(O_{2in} - O_{2out})} \times 100\%$$

where CO_{in} and CO_{out} describe the CO concentration in the inlet gas and gas leaving the reactor, respectively (similarly for $O_{2\,in}$ and $O_{2\,out}$).

3 Results and Discussions

3.1 Structure and Morphology

Three types of ceria support for gold nanoparticles were applied—CeO_2(NC), nanooctahedra CeO_2(NO), and nanofacetted nanocubes CeO_2(NF). Previously, we showed that CeO_2(NC), synthesized by the MAHT method, are single crystals, terminated by {100} faces, with a small contribution of {110} and {111} faces at the edges and corners, respectively [14, 18]. CeO_2(NO), also synthesized by the MAHT method, are single crystals terminated by {111} faces [1, 14, 19]. CeO_2(NF) are thermally reconstructed CeO_2(NC) with {110} faces transformed into zigzag structures of nanometer size {111} facets [14, 15].

Figure 1 shows the representative TEM images of as-prepared Au/CeO_2(NC) (Fig. 1a, d), Au/CeO_2(NF) (Fig. 1b, e) and Au/CeO_2(NO) (Fig. 1c, f) samples. ICP measurements show that Au content in Au/NC, Au/NO and Au/NF was 1.70, 1.77 and 1.68 wt% respectively. The experimental error of these measurements was 0.03 wt%. Thus we conclude, that Au content in all samples was the same. This result agrees with ~ 2 wt% Au contents measured by EDS.

Interestingly, the number of Au particles on zigzagged {111}-nanofacetted edges is higher than on the flat {110}-terminated edges of the unreconstructed CeO_2(NC) (cf. Figure 2a, b, d, e). It agrees well with a recent work of Fernández-García et al. [15], where the preferable Au deposition on the CeO_2(NF) support was observed. The authors explain it by higher anchoring capacity for gold during the deposition precipitation process on the reconstructed surface. In line with it, Lu et al. [21]. demonstrated that Au preferentially nucleates at the point defects and the step edges of {111} oriented CeO_2 film.

As seen in Table 1, the type of annealing atmosphere—reducing (H_2) and oxidative (air)) has a great impact on the growth of Au nanoparticles. Annealing of all the samples in air results in severe growth of Au nanoparticles. However, the reducing atmosphere (H_2) hindered the growth of Au particles in all investigated samples (cf. Table 1). We attribute it to the surface reduction of ceria during treatment of Au/ceria samples in H_2, and consequently to the formation of surface oxygen vacancies "anchors" sites for the Au nanoparticles.

Furthermore, the stability of Au nanoparticles depends on the type of ceria support's surface—{111} or {100}. The thermal stability of Au nanoparticles supported by flat {111} surface (nanooctahera) is higher than that on {100} one (nanocubes). Interestingly, Au nanoparticles supported by ceria nanooctahedra (terminated by {111} faces) demonstrate extremely high resistance to sintering in reducing

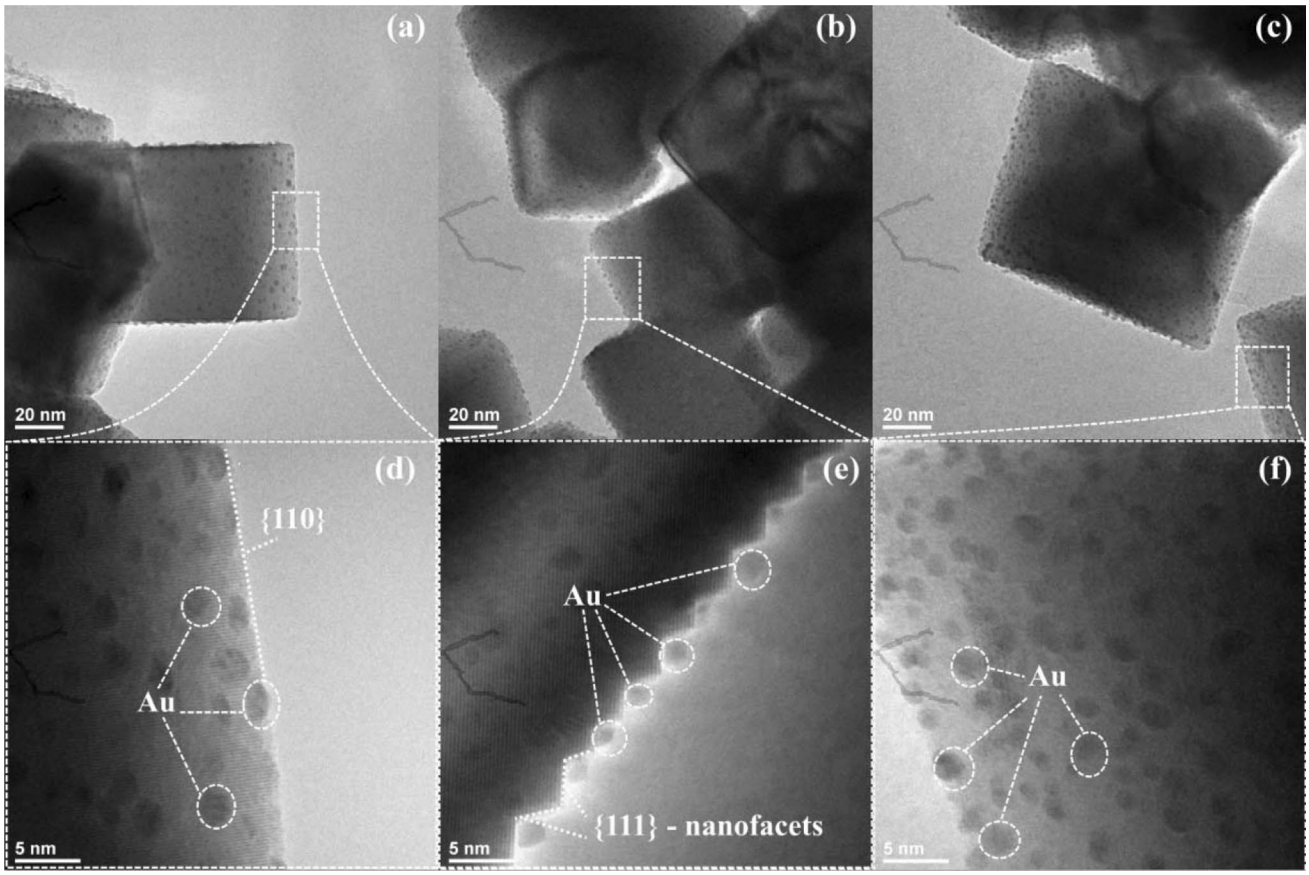

Fig. 1 TEM images of as-prepared Au/CeO_2(NC) (**a**, **d**), Au/CeO_2(NF) (**b**, **e**) and Au/CeO_2(NO) (**c**, **f**) samples

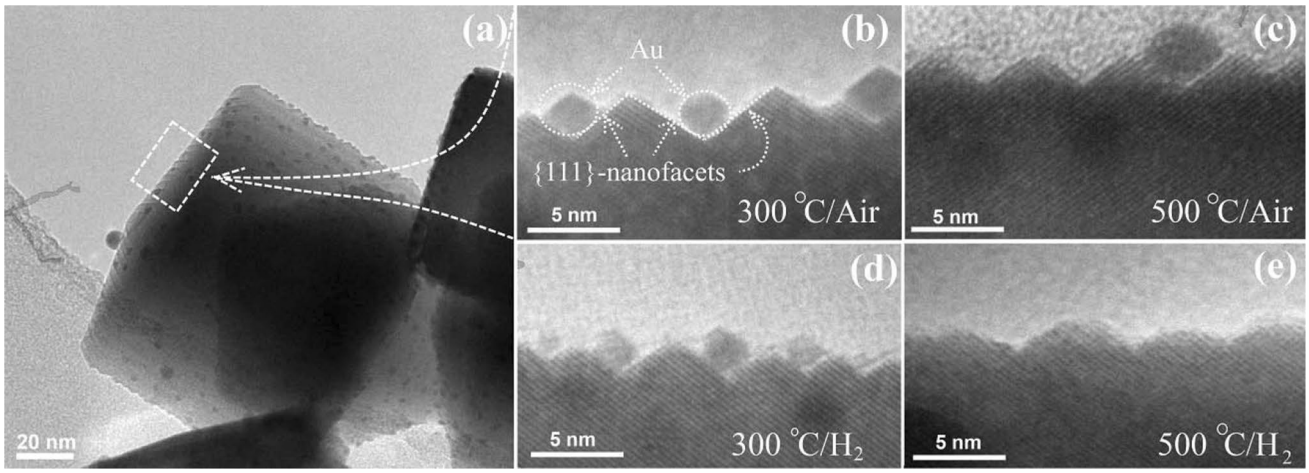

Fig. 2 TEM image of Au/CeO_2(NF) sample treated at 300 °C in air. HR-TEM images (recorded along [110] axis) of Au/CeO_2(NF) edges treated at 300 (**b**) and 500 °C (**c**) in air and at 300 (**d**) and 500 °C (**e**) in H_2

atmosphere—average sizes of Au nanoparticles in Au/CeO_2(NO) sample treated in H_2 at 500 °C is only 2 nm, while the average size of as-deposited Au nanoparticles is 1.5 nm. At first glance, Au nanoparticles should be more stable on {100} than {111} faces of CeO_2 because {100} faces contain more oxygen vacancies (potential "anchoring" sites) than {111}. Theoretical calculations showed that the energy of oxygen vacancy formation on

Table 1 The average size of Au nanoparticles in Au/CeO_2(NC), Au/CeO_2(NF), and Au/CeO_2(NO) samples before and after treatment in air and hydrogen at 300 and 500 °C (Au particle size distributions for all the samples are presented in ESI)

Sample	D(Au) average, nm					D(Au) average, on {111} nanofacets, nm				
	As prepared	300 °C		500 °C		As prepared	300 °C		500 °C	
		Air	*H_2*	*Air*	*H_2*		*Air*	*H_2*	*Air*	*H_2*
Au/CeO_2(NC)	1.7	2.4	*1.8*	8.4	*5.1*	–	–	–	–	–
Au/CeO_2(NO)	1.5	2.8	*1.8*	6.1	*2.0*	–	–	–	–	–
Au/CeO_2(NF)	1.6	2.3	*2.0*	6.0	*3.5*	1.6	*1.9*	*1.5*	*3–4*	–

the ceria surface is sensitive to the type of exposed lattice plane: {110} (+1.99 eV) < {100} (+2.27 eV) < {111} (+2.60 eV) [22, 23]. However, our data showed the opposite effect—Au nanoparticles are more stable on ceria nanooctahedra ((NO), terminated by {111} faces) than on nanocubes (NC) or reconstructed nanocubes ((NF), both mainly terminated by {100} faces). This apparent contradiction can be explained as follows. MD calculations by Castanet et al. showed that {111} surface of ceria does not undergo faceting nor reconstruction at any temperature, whereas the {100} surface has a very mobile (liquid-like) top layer with both the Ce and O ions being highly mobile [4]. It can be assumed that high ion mobility on the {100} surface inhibits "anchoring" of Au nanoparticles and creates favorable conditions for their sintering via Ostwald ripening mechanism.

Probably, the presence of phosphate impurities in Au/NO should also influence on sintering of Au nanoparticles. Futhermoere, phosphate impurities are most likely located on surface of nanooctahedra and can be "anchoring" sites for Au nanoparticles. However, this hypothesis requires an experimental verification.

It was found that gold nanoparticles appear to be more stable on zigzagged {111} nanofacetted surface than on flat {111} and relatively flat {110} surfaces both in oxidizing (air) and reducing atmosphere (H_2) (cf. Table 1). We attribute this to the inhibition of Ostwald ripening growth of Au nanoparticles on the zigzagged {111}-nanofacetted surface. Despite the absence of direct experimental confirmation, our hypothesis is in a good agreement with Lu et al. [21], who showed that the growth of Au particles proceeds mainly via atom diffusion along the steps on the CeO_2(111) support. In our case, the restriction of the surface diffusion of Au atoms to one direction along the "valleys" between nanofacets should inhibit the growth of Au particles.

The inhibitory effect of nanofaceted surface on the sintering of Au nanoparticles loses its efficiency at elevated temperatures. The representative TEM image of Au/CeO_2(NC) catalyst treated at 300 °C in the air is presented in Fig. 2a. As seen in Fig. 2b and d (recorded along [110] axis of ceria), numerous Au particles are present on zigzagged {111}-nanofacetted edges of the catalyst treated at 300 °C in air and H_2. However, the Au/CeO_2(NF) sample annealed at 500 °C in the air has a lower number of Au nanoparticles on {111} nanofacets than the same sample, treated both in air and H_2 at 300 °C (Fig. 2c). We assume that at this temperature, both Ostwald ripening and particle migration mechanisms may operate, and Au nanoparticles can migrate from {111} nanofacets toward flat {100} faces. It can explain their low-concentration on {111} nanofacets (which constitute approx. 10% of the total surface of NF). Annealing at 500 °C in H_2 results also in total degradation of zigzagged {111}-nanofacetted edges into more flatted and rounded structures (cf. Fig. 2e). The same transformation of {111}-nanofacetted structures on ceria nanorods into flat {110} surface was also observed by Crozier et al. [24]. Interestingly, {111}-nanofacetted structures on the edges of Au-free ceria nanocubes are stable at the same conditions (treatment 500 °C in H_2) [14]. Thus, it can be assumed that the presence of Au facilitates the {111}-nanofacets → flat {110} surface reconstruction under treatment in the reducing atmosphere. However, this supposition needs more in-depth investigation, which will be performed in our future work.

3.2 Reducibility

H_2-TPR is a powerful tool to provide information on the reducibility of ceria modified by metals. H_2-TPR profiles of Au/CeO_2(NC), Au/CeO_2(NF), and Au/CeO_2(NO) samples calcined at 300 °C and 500 °C are shown in Fig. 3. The profiles of all the samples can be divided into two regions: low (< 150 °C) and high (300–900 °C) temperature. Low-temperature H_2 consumption peaks (cf. Fig. 3) are related to the reduction of oxygen species on gold nanoparticles and to the surface reduction of ceria support [25–27]. A high-temperature broad peak (at 500–1000 °C) is typical for bulk reduction of ceria [18, 28, 29].

The broad peak (at 200–400 °C), observed exclusively for Au/CeO_2(NO) sample, is probably attributed to the reduction of phosphate impurities (Na_3PO_4 was used as a precipitant for CeO_2(NO) synthesis). However, this supposition needs experimental verification, which will be performed in our future work.

The low-temperature reducibility of Au/ceria samples, treated at 300 °C and 500 °C follows the sequence: Au/CeO_2(NC) > Au/CeO_2(NF) > Au/CeO_2(NO) and Au/

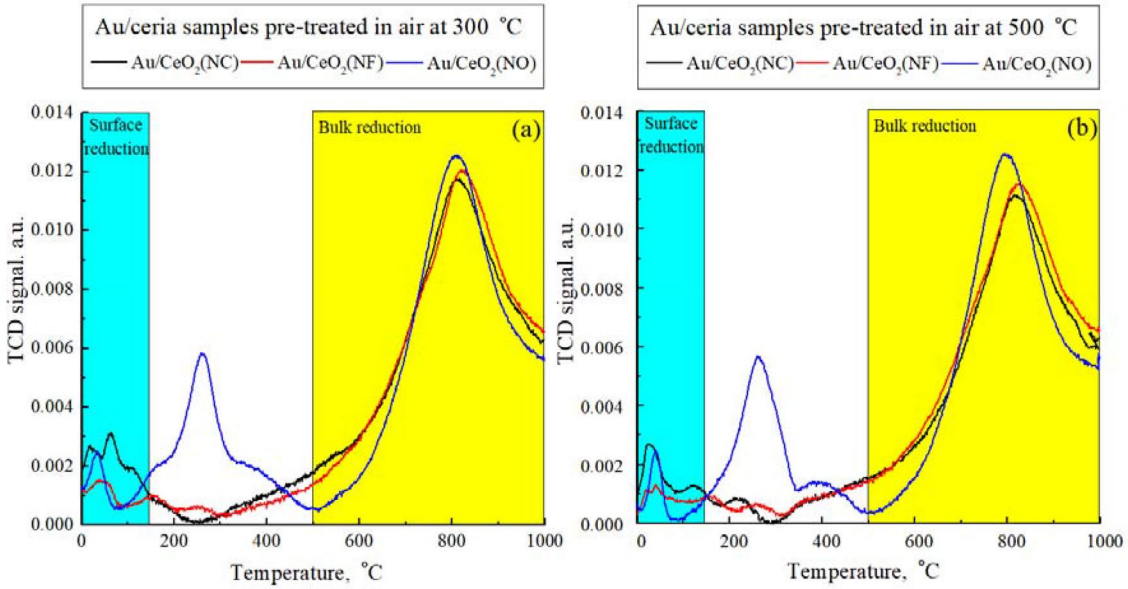

Fig. 3 H_2-TPR profiles of the Au/CeO_2(NC), Au/CeO_2(NF) and Au/CeO_2(NO) samples treated at 300 (**a**) and 500 °C (**b**) in air

Table 2 Low temperature H_2 consumption (0–150 °C temperature range) for Au/CeO_2(NC), Au/CeO_2(NF) and Au/CeO_2(NO) samples pre-treated at 300 and 500 °C

Sample	H_2 consumption, μmol	
	Pre-treated in air at 300 °C	Pre-treated in air at 500 °C
Au/CeO_2(NC)	4.68	3.29
Au/CeO_2(NF)	2.78	1.67
Au/CeO_2(NO)	2.22	1.88

The weights of the samples are 50 mg

CeO_2(NC) > Au/CeO_2(NO) > Au/CeO_2(NF), respectively. Rising the temperature of thermal pre-treatment in the air to 500 °C decreases the low-temperature reducibility of all samples by 15- 40% (see Table 2).

The effect of the morphology of ceria nanoparticles on the low-temperature reducibility of Au-ceria system can be explained in the following way. Ceria nanocubes, synthesized by the MAHT method, are single crystals, terminated by {100} faces, with a small contribution of {110} and {111} faces at the edges and corners, respectively [13, 14, 30]. Thus, the enhanced low-temperature reducibility of Au/CeO_2(NC) sample can be attributed to the low formation energy of oxygen vacancies at {100} and {110} faces [3].

Despite the same Au content in Au/CeO_2(NF) and Au/CeO_2(NC), the reducibility of Au/CeO_2(NF) is lower (by approx. 40%), both for the samples annealed at 300 and 500 °C. It appears that the edges of ceria nanocubes (which make < 10% of the total surface area) control the low-temperature reducibility (and accordingly reactivity) of Au/ceria system. In the case of CeO_2(NF), the active {110} surface on the edges is reconstructed to much less active {111} terminated nanofacets. In the literature, no H_2-TPR investigations of the reconstructed ceria nanocubes have been published yet. However, there are data regarding CeO_2(NF) and Au/CeO_2(NF) reactivity, which strongly correlates with the low-temperature reducibility of these materials. Our previous results show that the surface reconstruction of {110} terminated edges of ceria nanocubes results in a strong decrease in their catalytic reactivity in CO oxidation [14].

The decrease of the low-temperature reducibility with an increase of the treatment temperature up to 500 °C can be explained by a thermally induced growth (sintering) of gold nanoparticles. The average size of Au nanoparticles in Au/ceria samples, annealed at 300 and 500 °C is 2.3–2.8 and 6.0–8.4 nm, respectively (cf. Table 1). Thermally induced growth of Au nanoparticles reduces the number of easily reducible oxygen species on their surface, responsible for low-temperature H_2-TPR signal.

3.3 Catalytic Activity

3.3.1 CO-Oxidation

Figure 4 shows CO-oxidation light-off curves for Au/ceria samples. Since the specific surface area (SSA) of all the samples studied is comparable—14.6, 8.7 and 9.2 m^2/g for Au/CeO_2(NC), Au/CeO_2(NF) and Au/CeO_2(NO), respectively, it is admissible to conclude that variations in the catalytic

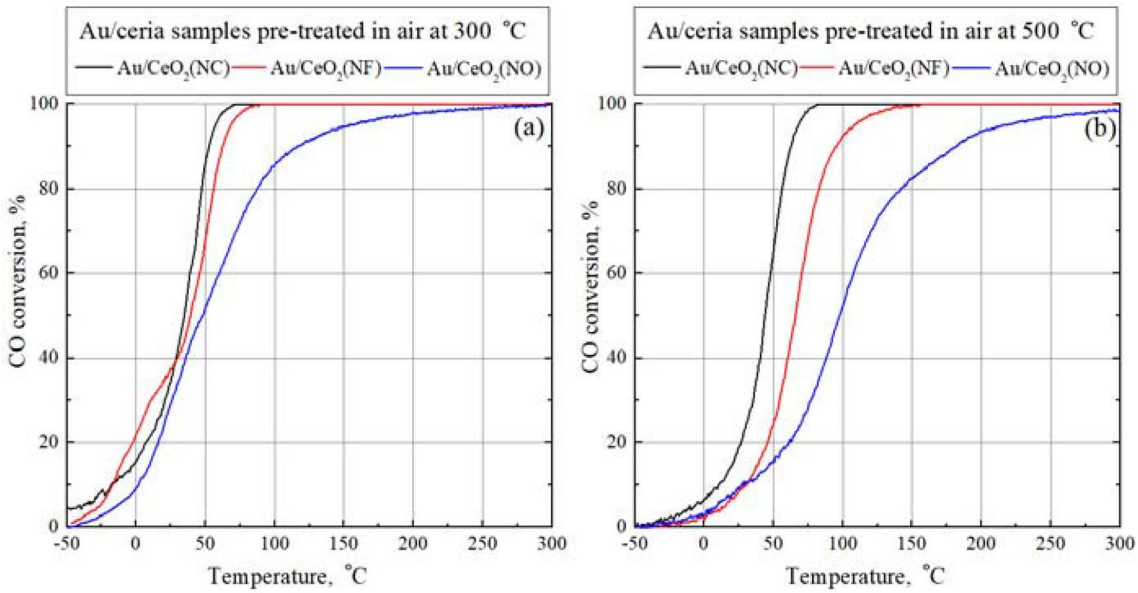

Fig. 4 CO oxidation light-off curves for the Au/CeO_2(NC), CeO_2(NF) and CeO_2(NO)samples treated at 300 (**a**) and 500 °C (**b**)

Table 3 T_{50} of Au/CeO_2(NC), Au/ CeO_2(NF), and Au/ CeO_2(NO) samples pre-treated at 300 and 500 °C

Sample	T_{50}, °C	
	300 °C	500 °C
Au/CeO_2(NC)	35	44
Au/CeO_2(NF)	39	66
Au/CeO_2(NO)	48	98

activity of the samples are determined mainly by the morphology of ceria support and the size of Au nanoparticles but not by the differences in the specific surface area. There is one more argument in favor of this assumption. The difference in SSA between Au/CeO_2(NC) and Au/CeO_2(NF) samples (caused by sintering of ceria nanocubes, which accompanies surface reconstruction of NC into NF) is maximum in all investigated samples. At the same time, these samples show similar catalytic activity (being inversely proportional to the temperature of half-conversion T_{50}) in CO oxidation (cf. Fig. 4; Table 3).

The catalytic activity (being inversely proportional to the temperature of half-conversion T_{50}) of the Au/ceria samples (annealed at 300 and 500 °C) follows the tendency: Au/CeO_2(NC) > Au/CeO_2(NF) > Au/CeO_2(NO). Interestingly, the difference in the catalytic activity is more pronounced for the samples, annealed at 500 °C.

Generally, the results on CO-oxidation correspond well with H_2-TPR data. Since the average sizes of Au nanoparticles supported on CeO_2(NC), CeO_2(NF) and CeO_2(NO) are comparable (see Table 1), we assume that the observed differences in catalytic activity are related to the details of the Au-ceria interface (which in turn depends on the morphology of ceria support). It is generally accepted that the perimeter sites at the gold-support interface are the active sites for low-temperature CO oxidation [5, 6].

The lowest activity of Au/CeO_2(NO) samples has two complementary explanations. The first is a low reactivity of the {111} surfaces terminating the ceria nanooctehedra [3]. The second is a presence of phosphorous (due to the use of Na_3PO_4 as a precipitant during ceria CeO_2(NO) synthesis). Phosphorous inhibits oxygen diffusion within the subsurface region of CeO_2 [31], and in consequence, lowers the catalytic activity of ceria.

The explanation of the differences in the catalytic activity of Au/CeO_2(NC) and Au/CeO_2(NF) samples is more complicated. Au/CeO_2(NC), pre-treated at both temperatures (300 and 500 °C) is more active than Au/CeO_2(NF) annealed at the same temperatures (Fig. 4; Table 3). We attribute the higher activity of Au/CeO_2(NC) sample to the gold particles located at highly active {110} faces on edges of ceria nanocubes. The activity of Au/CeO_2(NF) samples is lower due to the lower reactivity of gold particles located on {111}-nanofacets, created by reconstruction of {110} faces on NCs edges. This hypothesis is in a good agreement with our previous finding that bare CeO_2(NC) are more active in CO-oxidation than CeO_2(NF) [14]. Moreover, using Raman spectroscopy, we found that the concentration of oxygen defects in CeO_2(NC) sample is higher than in CeO_2(NF) [14].

On the other hand, Tinoco et al. showed that gold supported on the CeO_2(NF) presents an intrinsic (per gold surface atom) CO oxidation activity much higher than gold on the non-reconstructed oxide [13]. Fernández-García et al.,

attribute it to the presence of peroxide surface species (O_2^{2-}) at {111} nanofacets [15]. Despite this contradiction, which we cannot explain at this moment, an important role of the texture of the edges of ceria nanocubes is clearly visible.

However, the difference in activity of various samples treated at 300 and 500 °C is not as significant as one would expect, considering distinct average sizes of gold nanoparticles. It can be explained by the presence of highly active sub-nanometer Au nanoclusters in pre-treated samples (both at 300 and 500 °C). In our previous works, we observed, using (S)TEM technique, such Au clusters in Au/CeO_2(NC) annealed at 300 °C [32, 33]. The second possible explanation is the presence of pseudo-single sites, i.e., gold ions slightly abstracted from a gold clusters, which exhibit lower activation energy in the rate-determining step of CO-oxidation [34]. However, these hypotheses require HR-(S)TEM + DRIFTS + DFT verification, which we are going to do in further study.

3.3.2 CO PROX

The activity and selectivity of various Au/CeO_2 samples in CO PROX are compared in Fig. 5a and b. For all samples, the CO conversion first increases with the reaction

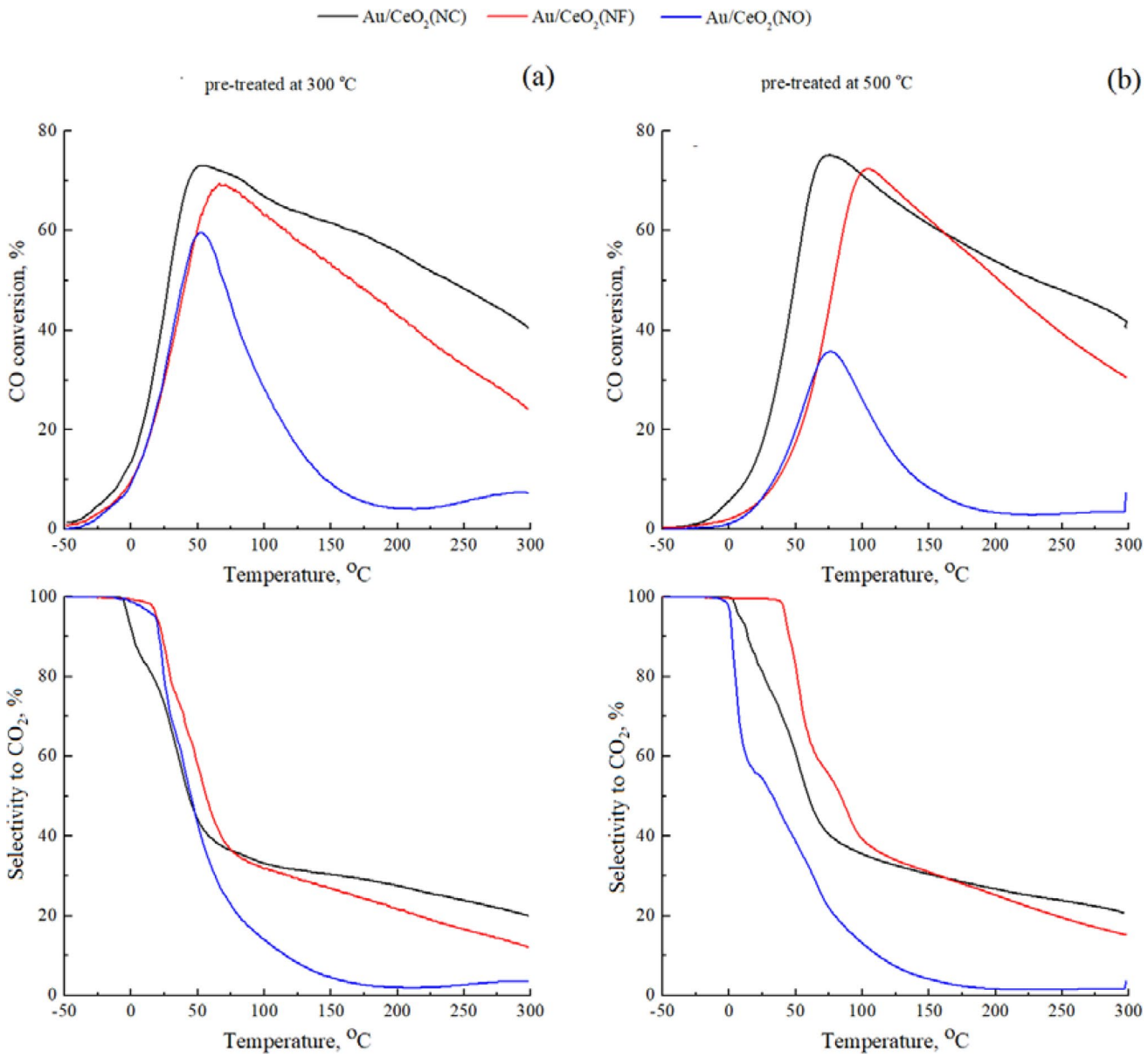

Fig. 5 Temperature-programmed reaction of CO PROX over Au/CeO_2(NC), Au/CeO_2(NF) and Au/CeO_2(NO) samples treated at 300 (**a**) and 500 °C (**b**)

temperature to a maximum at 50–100 °C, and then it decreases (Fig. 5a, b-top). Characteristic temperatures of half conversion—T1 (growth) and T2 (decline) are summarized in Table 4. Figure 5a and b—bottom show that selectivity of all samples strongly decreases with increasing reaction temperature to ~ 35% at 50–70 °C. Further growth of the reaction temperature to 300 °C lowers the selectivity to 20% or less (Fig. 4). The numerical values of selectivity at T_{50} and temperatures when 50% selectivity is obtained ($T(S_{50\%})$) of $Au/CeO_2(NC)$, $Au/CeO_2(NF)$ and $Au/CeO_2(NO)$ samples annealed at various temperatures (300 and 500 °C) are summarized in Table 4.

Generally, the results of CO-PROX correspond with CO-oxidation and H_2-TPR data, but there are some differences. As seen in Table 4, the catalytic activity (being inversely proportional to the minimal (T1) temperature of half-conversion T_{50}) of Au/ceria samples (annealed at 300 and 500 °C) in CO PROX follows the tendency: $Au/CeO_2(NC) > Au/CeO_2(NF) \approx Au/CeO_2(NO)$. Nevertheless, the catalytic activity of the samples in CO-oxidation follows the sequence $Au/CeO_2(NC) > Au/CeO_2(NF) > Au/CeO_2(NO)$. The observed difference indicates that the reconstruction of {110} surfaces at the edges of ceria nanocubes into zigzagged {111} structure more strongly declines the efficiency of CO oxidation in H_2 stream.

The width (T1–T2) of temperature window of the efficient CO oxidation (CO conversion > 50%) follows the sequence: $Au/CeO_2(NC) > Au/CeO_2(NF) > > Au/CeO_2(NO)$. As seen in Table 4, the selectivity of the samples at minimal (T1) temperature of T_{50} follows the tendency: $Au/CeO_2(NC) \approx Au/CeO_2(NF) > Au/CeO_2(NO)$. It shows that both parameters are the worst for $Au/CeO_2(NO)$. The $Au/CeO_2(NF)$ sample (annealed at 300 and 500 °C) maintain relatively high selectivity (50%) to a higher temperature as compared to other samples. Most likely, the structure of the edges of ceria nanocubes does not influence on the selectivity of Au/ceria catalysts in CO oxidation.

The catalytic performance of all investigated samples decreases with the increase of the pre-treatment temperature from 300 to 500 °C. As we mentioned above, it is, most likely, attributed to the sintering of Au nanoparticles and, as a consequence—decreasing the number of active sites.

As already mentioned, the CO conversion curves for each sample had similar characteristics. After the initial rapid increase to a maximum value at 50–100 °C, a decrease with a further rise of temperature was observed. The decline of the CO conversion in CO PROX at temperatures above 50–100 °C is related to two processes: competitive oxidation of hydrogen and desorption of carbon monoxide from gold nanoparticles. Oxidation of carbon monoxide and hydrogen on gold catalysts takes place at the same active centers, which are located at the metal support perimeter and low-coordinated gold atoms [35, 36]. This means that CO and H_2 compete for access to the same active centers of the catalyst. At low temperatures, when the strength of CO adsorption on gold nanoparticles is relatively high, the CO oxidation prevails. As the reaction temperature increases, CO surface coverage on gold nanoparticles decreases, and oxidation of hydrogen is more efficient [37] (it should be remembered that the concentration of H_2 is much higher than that of CO). Since the amount of oxygen in the CO PROX reaction is limited, most of the oxygen can be consumed by H_2 oxidation when the hydrogen oxidation yield is too high, and CO conversion starts to decrease. In our case, the oxygen concentration in the feed gas is 1%, so the oxygen deficiency for CO oxidation occurs when the selectivity to CO_2 is lower

Table 4 A comparison of $Au/CeO_2(NC)$, $Au/CeO_2(NF)$, and $Au/CeO_2(NO)$ catalysts in their performance and selectivity for CO PROX

Sample		CO oxidation				
		T_{50}, °C		Selectivity at T_{50}, %		$T_{(S50\%)}$, °C
		T1	T2	T1	T2	
$Au/CeO_2(NC)$	300 °C	28	239	70	25	43
	500 °C	50	231	62	25	61
$Au/CeO_2(NF)$	300 °C	41	166	67	25	56
	500 °C	79	203	53	25	84
$Au/CeO_2(NO)$	300 °C	40	69	58	26	44
	500 °C	–		–		32

T_{50} (T1)—temperature of half conversion in the ascending section of the CO-oxidation curve (other words – minimal temperature of half conversion)

T_{50} (T2)—temperature of half conversion in the downward section of the CO-oxidation curve

Selectivity at T_{50}(T1)—selectivity at the temperature of half conversion in the ascending section of the CO-oxidation curve T_{50}(T1)

Selectivity at T_{50}(T2)—selectivity at the temperature of half conversion in the downward section of the CO-oxidation curve T_{50}(T2)

$T_{(S50\%)}$—temperature when selectivity downwards to 50%

than 50% (assuming total conversion of oxygen). As can be seen in Fig. 4, for most samples, CO conversion starts to decrease around the temperature when the PROX selectivity reaches about 50%.

From a practical point of view, the optimal CO-PROX reaction temperature is around 100 °C, which corresponds to the operating temperature of the PEM fuel cell [38]. It is believed that restriction of the activity of Au/CeO_2 catalysts in the hydrogen oxidation in this temperature range is necessary to increase their selectivity in the CO-PROX reaction. [39, 40].

The selectivity of the tested catalysts depends on both the morphology of the ceria support and the size of the gold nanoparticles (related to the temperature of the thermal pre-treatment in the air). Comparing the selectivity of the catalysts pre-treated at 300 °C in the air (Fig. 4), it is seen that the selectivity of the Au/CeO_2(NO) catalyst above 50 °C is much lower than the other samples. The growth of gold nanoparticles after thermal pre-treatment at 500 °C in the air, leads to a decrease in the activity of all the catalysts. In summary, the Au/CeO_2(NO) catalyst not only showed the lowest activity in CO oxidation among the studied samples but also the lowest selectivity in PROX reaction. It can be explained as follows. The size of gold nanoparticles was comparable in all three catalysts (cf. Table 1). It remains an open question about the presence/absence of highly active subnanometer Au clusters in these samples. However, we observed the presence of such Au clusters in Au/CeO_2(NC) annealed at 300 °C [32, 33]. There are no objective reasons which can prevent thermally induced redispersion (e.g., strong anchoring on oxygen vacancies) in all investigated samples (annealed in the air only). Hence it is logical to assume that the fraction of highly active subnanometer Au clusters occurs in all investigated samples also. Thus, it can be stated that the type of the exposed ceria faces (and probably, presence/absence of phosphorous) had a decisive influence on the Au/CeO_2(NO) catalyst selectivity in PROX.

4 Conclusions

The sintering of Au nanoparticles on three types of ceria support (nanocubes (NC), nanooctahedra (NO), and nanofacetted nanocubes (NF)) has been investigated. It was shown that the thermal stability of Au nanoparticles supported by flat {111} and {100} surfaces of ceria is similar. Still, gold nanoparticles appear to be most stable on zigzagged {111} nanofacetted surface, formed by the reconstruction of {110} surfaces at the edges of ceria nanocubes. The smaller size of Au particles in the latter sample has, however, no noticeable effect on the catalytic activity in CO—oxidation and CO PROX. Moreover, Au/CeO_2(NF) sample shows lower reactivity and selectivity in CO oxidation in comparison to Au/CeO_2(NC). Therefore, ceria nanocubes with flat edges terminated by {110} surfaces appear more suitable as a support for Au nanoparticles, used to catalyze CO oxidation, than {111} nanofacetted ceria nanocubes.

Acknowledgements This work was financially supported by NCN (UMO-2017/27/N/ST5/02731). The authors thank Dr. K. Adamska for BET measurements and Dr. D. Szymanski for EDS measurements and prof. Pohl for ICP measurements.

Compliance with Ethical Standards

Conflict of interest The authors declare that they have no conflict of interest.

References

1. Trovarelli A, Llorca J (2017) Ceria catalysts at nanoscale: how do crystal shapes shape catalysis? ACS Catal 7:4716–4735
2. Schubert MM, Hackenberg S, Van Veen AC, Muhler M, Plzak V, Behm RJ (2001) CO Oxidation over supported gold catalysts—"inert" and "active" support materials and their role for the oxygen supply during reaction. J Catal 197:113–122
3. Conesa JC (1995) Computer modeling of surfaces and defects on cerium dioxide. Surf Sci 339:337–352
4. Castanet U, Feral-Martin C, Demourgues A, Neale RL, Sayle DC, Caddeo F, Flitcroft JM, Caygill R, Pointon BJ, Molinari M, Majimel J (2019) Controlling the 111}/{110 surface ratio of cuboidal ceria nanoparticles. Mater Interfaces 11:11384–11390
5. Fujitani T, Nakamura I (2011) Mechanism and active sites of the oxidation of CO over Au/TiO2. Angew Chem Int Ed 50:10144–10147
6. Ta N, Liu J, Chenna S, Crozier PA, Li Y, Chen A, Shen W (2012) Stabilized gold nanoparticles on ceria nanorods by strong interfacial anchoring. J Am Chem Soc 134:20585–20588
7. He J, Kunitake T (2004) Preparation and thermal stability of gold nanoparticles in silk-templated porous filaments of titania and zirconia. Chem Mater 16:2656–2661
8. Liu S, Xu W, Niu Y, Niu Y, Zhang B, Zheng L, Liu W, Li L, Wang J (2019) Ultrastable Au nanoparticles on titania through an encapsulation strategy under oxidative atmosphere. Nat Commun 10:5790
9. Saxena S, Singh R, Pala RGS, Sivakumar S (2016) Sinter-resistant gold nanoparticles encapsulated by zeolite nanoshell for oxidation of cyclohexane. RSC Adv 6:8015–8020
10. Ruckenstein E, Pulvermacher B (1973) Kinetics of crystallite sintering during heat treatment of supported metal catalysts. AIChE J 19:356–364

11. Behafarid F, Cuenya RB (2013) Towards the understanding of sintering phenomena at the nanoscale: geometric and environmental effects. Top Catal 56:1542–1559
12. Fronzi M, Soon A, Delley B, Traversa E, Stampfl C (2009) Stability and morphology of cerium oxide surfaces in an oxidizing environment: a first-principles investigation. J Chem Phys 131:104701
13. Tinoco M, Fernandez-Garcia S, Lopez-Haro M, Hungria AB, Chen X, Blanco G, Perez-Omil JA, Collins SE, Okuno H, Calvino JJ (2015) Critical influence of nanofaceting on the preparation and performance of supported gold catalysts. ACS Catal 5:3504–3513
14. Bezkrovnyi OS, Kraszkiewicz P, Ptak M, Kepinski L (2018) Thermally induced reconstruction of ceria nanocubes into zigzag {111}-nanofacetted structures and its influence on catalytic activity in CO oxidation. Catal Commun 117:94–98
15. Fernández-García S, Collins SE, Tinoco M, Hungría AB, Calvino JJ (2019) Influence of 111 nanofaceting on the dynamics of CO adsorption and oxidation over Au supported on CeO2 nanocubes: an operando DRIFT insight. Catal Today 336:90–98
16. Dong C, Zhou Y, Ta N, Shen W (2020) Formation mechanism and size control of ceria nanocubes. CrystEngComm. https://doi.org/10.1039/d0ce00224k
17. Bezkrovnyi OS, Lisiecki R, Kepinski L (2016) Relationship between morphology and structure of shape-controlled CeO2 nanocrystals synthesized by microwave-assisted hydrothermal method. Cryst Res Technol 51:554–560
18. Bezkrovnyi O, Małecka MA, Lisiecki R, Ostroushko V, Thomas AG, Gorantla S, Kepinski L (2018) The effect of Eu doping on the growth, structure and red-ox activity of ceria nanocubes. CrystEngComm 20:1698–1704
19. Małecka MA (2017) Characterization and thermal stability of Yb-doped ceria prepared by methods enabling control of the crystal morphology. CrystEngComm 19:6199–6207
20. Lin Y, Wu Z, Wen J, Ding K, Yang X, Poeppelmeier KR, Marks LD (2015) Adhesion and atomic structures of gold on ceria nanostructures: the role of surface structure and oxidation state of ceria supports. Nano Lett 15:5375–5381
21. Lu JL, Gao HJ, Shaikhutdinov S, Freund HJ (2007) Gold supported on well-ordered ceria films: nucleation, growth and morphology in CO oxidation reaction. Catal Lett 114:8–16
22. Nolan M, Parker SC, Watson GW (2005) The electronic structure of oxygen vacancy defects at the low index surfaces of ceria. Surf Sci 595:223–232
23. Nolan M, Fearon JE, Watson GW (2006) Oxygen vacancy formation and migration in ceria. Solid State Ion 177:3069–3074
24. Crozier PA, Wang R, Sharma R (2008) In situ environmental TEM studies of dynamic changes in cerium-based oxides nanoparticles during redox processes. Ultramicroscopy 108:1432–1440
25. Fu Q, Weber A, Flytzani-Stephanopoulos M (2001) Nanostructured Au–CeO_2 catalysts for low-temperature water–gas shift. Catal Lett 77:87–95
26. Zhang Y, Zhao Y, Zhang H, Zhang L, Ma H, Dong P, Li D, Yu J, Cao G (2016) Investigation of oxygen vacancies on Pt- or Au modified CeO_2 materials for CO oxidation. RSC Adv 6:70653–70659
27. Wang XL, Fu XP, Wang WW, Ma C, Si R, Jia CJ (2019) Effect of structural evolution of gold species supported on ceria in catalyzing CO oxidation. J Phys Chem C 123:9001–9012
28. Xu JH, Harmer J, Li GQ, Chapman T, Collier P, Longworth S, Tsang SC (2010) Size dependent oxygen buffering capacity of ceria nanocrystals. Chem Commun 46:1887–1889
29. Wang XY, Wang SP, Wang SR, Zhao YQ, Huang J, Zhang SM, Huang WP, Wu SH (2006) The preparation of Au/CeO_2 catalysts and their activities for low-temperature CO oxidation. Catal Lett 112:115–119
30. Florea I, Feral-Martin C, Majimel J, Ihiawakrim D, Hirlimann C, Ersen O (2013) Three-dimensional tomographic analyses of CeO_2 nanoparticles. Cryst Growth Des 13:1110–1121
31. Granados ML, Galisteo FC, Lambrou PS, Mariscal R, Sanz J, Sobrados I, Fierro JLG, Efstathiou AM (2006) Role of P-containing species in phosphated CeO_2 in the deterioration of its oxygen storage and release properties. J Catal 239:410–421
32. Bezkrovnyi O, Kraszkiewicz P, Krivtsov I, Quesada J, Ordóñez S, Kepinski L (2019) Thermally induced sintering and redispersion of Au nanoparticles supported on $Ce_{1-x}Eu_xO_2$ nanocubes and their influence on catalytic CO oxidation. Catal Commun 131:105798
33. Bezkrovnyi OS, Blaumeiser D, Vorokhta M, Kraszkiewicz P, Pawlyta M, Bauer T, Libuda J, Kepinski L (2020) NAP-XPS and in-situ DRIFTS of the interaction of CO with Au nanoparticles supported by $Ce_{1-x}Eu_xO_2$ nanocubes. J Phys Chem C. https://doi.org/10.1021/acs.jpcc.9b10142
34. Schilling C, Ziemba M, Hess C, Ganduglia-Pirovano MV (2020) Identification of single-atom active sites in CO oxidation oxoxide-supported Au catalysts. J Catal 383:264–272
35. Widmann D, Hocking E, Behm RJ (2014) On the origin of the selectivity in the preferential CO oxidation on Au/TiO2 – Nature of the active oxygen species for H_2 oxidation. J Catal 317:272–276
36. Wang LC, Widmann D, Behm RJ (2015) Reactive removal of surface oxygen by H_2, CO and CO/H_2 on a Au/CeO_2 catalyst and its relevance to the preferential CO oxidation (PROX) and reverse water gas shift (RWGS) reaction. Catal Sci Technol 5:925–941
37. Schubert MM, Kahlich MJ, Gasteiger HA, Behm RJ (1999) Correlation between CO surface coverage and selectivity/kinetics for the preferential CO oxidation over Pt/γ-Al2O3 and Au/α-Fe2O3: an in-situ DRIFTS study. J Power Sour 84:175–182
38. Mehta V, Cooper JS (2003) Review and analysis of PEM fuel cell design and manufacturing. J Power Sour 114:32–53
39. Lakshmanan P, Park JE, Park ED (2014) Recent advances in preferential oxidation of CO in H2 over gold catalysts. Catal Surv Asia 18:75–88
40. Centeno MA, Reina TR, Ivanova S, Laguna OH, Odriozola JA (2016) Au/CeO2 catalysts: structure and CO oxidation activity. Catalysts 6(158):1–30

Affiliations

O. S. Bezkrovnyi[1] · P. Kraszkiewicz[1] · W. Mista[1] · L. Kepinski[1]

✉ O. S. Bezkrovnyi
O.Bezkrovnyi@intibs.pl

[1] W. Trzebiatowski Institute of Low Temperature and Structure Research Polish Academy of Sciences, Wrocław, Poland